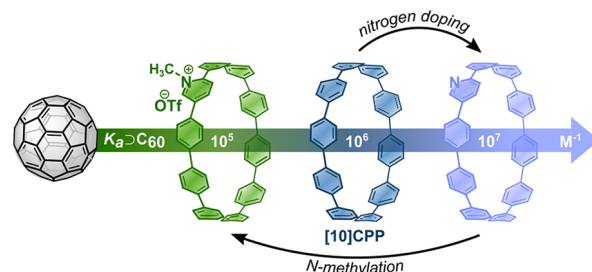


Synthesis and C₆₀ Binding of Aza[10]CPP and *N*-Methylaza[10]CPP

Fabian Schwer^aSimon Zank^b Markus Freiburger^bRamandeep Kaur^bStefan Frühwald^cCraig C. Robertson^dAndreas Görling^cThomas Drewello^{*b} Dirk M. Guldi^{*b} Max von Delius^{*a} ^a Institute of Organic Chemistry, Ulm University,
Albert-Einstein-Allee 11, 89081 Ulm, Germany.^b Department of Chemistry and Pharmacy, Physical Chemistry I,
Friedrich-Alexander Universität Erlangen-Nürnberg,
Egerlandstrasse 3, 91058 Erlangen, Germany.^c Department of Chemistry and Pharmacy, Theoretical Chemistry,
Friedrich-Alexander Universität Erlangen-Nürnberg,
Egerlandstrasse 3, 91058 Erlangen, Germany.^d Department of Chemistry, University of Sheffield, Brook Hill,
Sheffield S3 7HF, U.K.* max.vondelius@uni-ulm.de; dirk.guldi@fau.de;
thomas.drewello@fau.de

Received: 13.01.2022

Accepted after revision: 10.03.2022

DOI: 10.1055/a-1814-7686; Art ID: OM-2022-01-0001-OA

License terms:

© 2022. The Author(s). This is an open access article published by Thieme under the terms of the Creative Commons Attribution License, permitting unrestricted use, distribution, and reproduction so long as the original work is properly cited. (<https://creativecommons.org/licenses/by/4.0/>).

Abstract Within the growing family of strained carbon nanohoops and nanobelts, [10]CPP arguably offers the best compromise between synthetic accessibility and strong binding affinity for C₆₀. In this work, we report the synthesis of two nitrogen-containing analogues of [10]CPP and we systematically compare the structure, optoelectronic properties and C₆₀ binding affinities of this small set of structurally similar macrocycles. While Aza[10]CPP outcompetes the parent compound by approximately one order of magnitude with respect to C₆₀ binding, we found that the reverse was true for the methylaza analogue. Transient absorption studies showed that photo-induced electron transfer occurred readily from [10]CPP and its aza-analogue to an encapsulated C₆₀ guest. Formation of a charge-separated complex was not observed however for the *N*-methylated derivative. These insights will prove useful for further applications of strained nanohoops in supramolecular chemistry and organic electronics.

Key words: curved π -systems, host–guest chemistry, fullerenes, nitrogen doping, photo-induced electron transfer

Introduction

The synthesis of strained carbon nanohoops¹ and nanobelts² has received much attention since Jasti's report of the first [n]cycloparaphenylenes ([n]CPPs) in 2008.³ Inspired by their unusual optoelectronic^{1b,4} and supramolecular properties⁵, researchers have made structural variations to the CPP framework. These variations include the introduction of larger π -fragments⁶ and electron-donating or withdrawing⁷ moieties within the ring as well as the installation of peripheral halide atoms⁸ and larger (bridging) substituents.^{8e,9} CPPs with more complex topologies have also been pursued, most notably a trefoil knot,¹⁰ cages¹¹ and figure-eight macrocycles.¹² Due to our interest in the encapsulation of fullerenes within nanohoops,^{8e,9o,t,z,ae,13} the introduction of heteroatoms into the core CPP framework is a particularly appealing method of variation.¹⁴ We were therefore surprised that no aza-derivatives of [10]CPP, as the ideal CPP host for C₆₀, were reported.

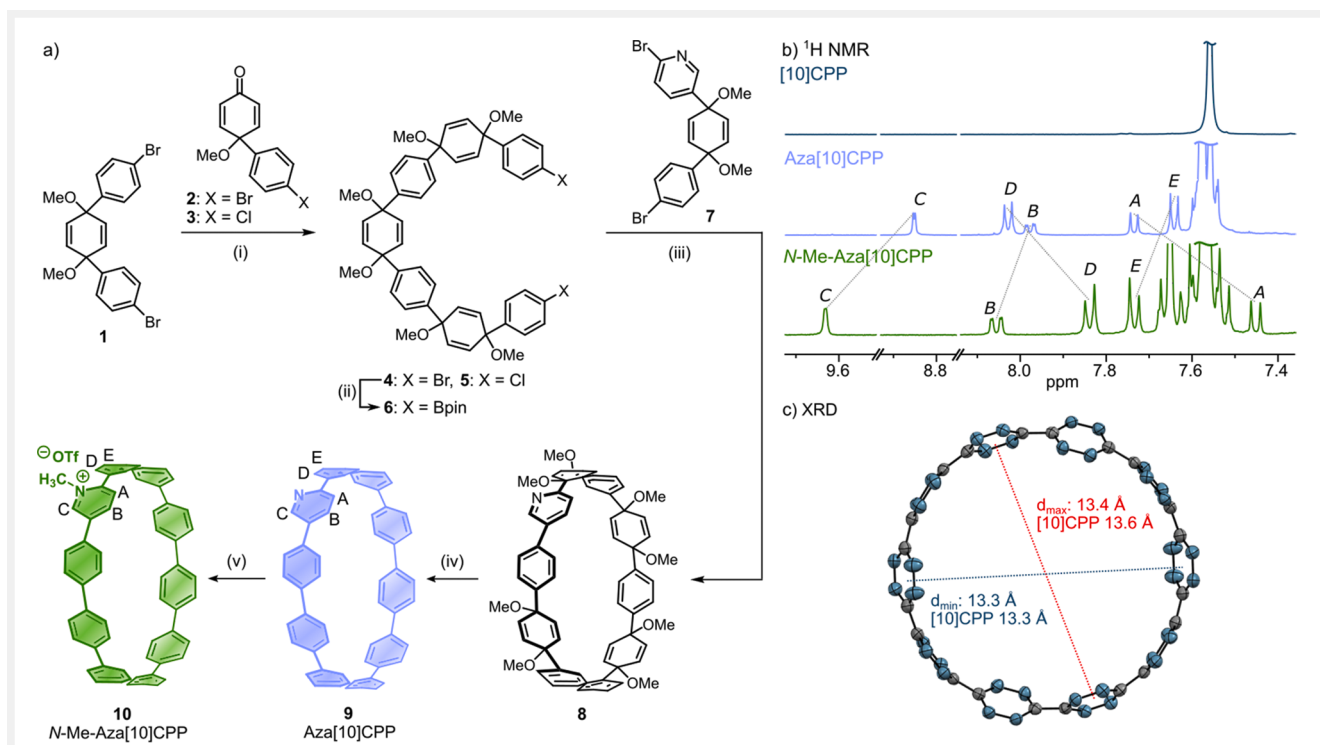
In this work, we describe the synthesis of Aza[10]CPP and its *N*-methylated derivative *N*-Me-Aza[10]CPP. In a systematic supramolecular study in solution and in the gas phase, we compared the binding affinities between the three related hosts and C₆₀ as a guest. Motivated by recent studies on the use of CPPs as organic semiconductors¹⁵ and mediators of charge transfer,^{8e} we also investigated the optoelectronic properties of the new compounds as well as their C₆₀ complexes in the ground state and the excited state.

Results and Discussion

To prepare the aza-analogue of [10]CPP, we decided to make use of a procedure developed by Jasti and coworkers for the synthesis of Aza[6]CPP and Aza[8]CPP (Scheme 1).^{14b,c} The conventional, i.e. carbon- and hydrogen-based, part of the macrocycle was synthesized from compound **1** via two-fold lithium-halogen exchange, followed by reaction with 2 equiv of ketones **2** or **3**, yielding the U-shape dibromide **4** or dichloride **5**, respectively. Dibromide **4** was converted into boronic ester **6** in 78% yield by another lithium-halogen exchange followed by treatment with *i*-PrO-Bpin. The pathway via dichloride **5** also proceeds with approx. 80% yield and requires Suzuki-Miyaura conditions with reagent Bpin₂ to furnish the same product. Pyridine-containing dibromide **7** (prepared exactly as described by Jasti^{14b}) and boronic ester **6** were subsequently coupled under highly dilute Suzuki-Miyaura conditions. At this stage, a mixture of (mainly) cyclic products was treated with freshly prepared sodium naphthalenide to give Aza[10]CPP **9** in a two-step yield of 9% after column chromatography. Using the highly

reactive reagent methyl triflate, we were able to convert Aza[10]CPP **9** into *N*-Me-Aza[10]CPP triflate **10** in an optimized yield of 89%. For further details on synthesis, please refer to the Supporting Information.

While [10]CPP shows only one signal in the ¹H NMR spectrum, the single nitrogen atom in Aza[10]CPP leads to desymmetrization and therefore a more complex spectrum (Scheme 1b), in which the chemical shifts of the protons of the pyridyl moiety (A, B and C) differ significantly from those found in [10]CPP. After methylation, protons B and C are shifted downfield (Scheme 1b, green) and proton A is shifted upfield as a result of their relative position to the quaternized nitrogen atom. We were able to obtain single crystals of Aza[10]CPP suitable for X-ray crystallography by slow evaporation of a dilute solution in chloroform. We found that the single nitrogen atom within the macrocycle of Aza[10]CPP (molecular formula: C₅₉H₃₉N) is disordered over all 40 possible isosteric positions (see Scheme 1c). This observation was previously also made by Jasti for compounds Aza[8]CPP and Aza[6]CPP.^{14b,c} Compared to the published solid-state structure of [10]CPP,¹⁶ Aza[10]CPP is a little more



Scheme 1 a) Synthesis of Aza[10]CPP **9** and *N*-Me-Aza[10]CPP **10**. Conditions: (i) 1. *n*-BuLi, THF, -78 °C. 2. **2/3**. 3. NaH, MeI, THF, 0 °C, **2**: 70 %, **3**: 46 %. (ii) **4**: 1. *n*-BuLi, THF, -78 °C. 2. *i*-PrO-Bpin, 78 %. **5**: Bpin₂, Pd(OAc)₂, SPhos, K₃PO₄, 1,4-dioxane, 90 °C, 81 %. (iii) Pd(PPh₃)₄, (*n*-Bu)₄NBr, NaHCO₃, MePh/MeOH/H₂O 17:2:1, 90 °C. (iv) Sodium naphthalenide, THF, -78 °C, 9 % over two steps. (v) MeOTf, DCM, 89 %. b) Partial ¹H NMR spectra (CDCl₃, 400 MHz) of [10]CPP (in dark blue, measured at 298 K), Aza[10]CPP (**9**) (in bright blue, measured at 340 K) and *N*-Me-Aza[10]CPP **10** (in green, measured at 298 K). c) Solid-state structure and minimal/maximal diameters of Aza[10]CPP **9**. Crystal system: monoclinic; space group: P2₁/c. Black atoms refer to carbon. Blue atoms refer to the electron density of 1/40 N and 39/40 C.

“round” since its minimal and maximal diameters are nearly identical ($d_{\min} = 13.3 \text{ \AA}$ and $d_{\max} = 13.4 \text{ \AA}$, Scheme 1c), whereas in [10]CPP there is a somewhat more pronounced difference ($d_{\min} = 13.3 \text{ \AA}$ and $d_{\max} = 13.6 \text{ \AA}$). Because it would explain the higher binding affinity for C_{60} (*vide infra*), we propose that this rounder shape also exists in solution, even though we cannot exclude that the effect is caused by the disorder on nitrogen or packing in the solid state. Moreover, we observed a slightly smaller average torsional angle (the angle about which two adjacent phenylenes are tilted) of Aza[10]CPP ($\theta_0 = 26.5^\circ$) compared to [10]CPP ($\theta_0 = 26.9^\circ$) in the crystal structure. This trend was also found in density functional theory (DFT) calculations (*vide infra*). Despite our best efforts using different methods, we were unable to grow single crystals of *N*-Me-Aza[10]CPP.

To delve deeper into all three molecular structures and gather evidence that is independent of packing effects, we carried out DFT calculations of Aza-, *N*-Me-Aza- and the parent [10]CPP (level of theory: B3LYP/6-31 G(d)+D3); for further details see the Supporting Information). An interesting parameter for [n]CPPs is the torsional angle between two phenylene moieties because it is affected by repulsive steric interactions of the *ortho*-hydrogen atoms on the one hand and by the amount of internal (macrocyclic) strain on the other hand. Replacing one carbon by one nitrogen atom and thereby replacing one hydrogen atom with a lone pair led to flattening of the Aza[10]CPP ($\theta_0 = 25.6^\circ$) compared to [10]CPP ($\theta_0 = 27.3^\circ$). This observation is consistent with studies of Stück and co-worker who theoretically examined heteroatom-substituted nanohoops.¹⁷ As expected, the additional methyl group in *N*-Me-Aza[10]CPP is more sterically demanding than a hydrogen atom and therefore results in an increased average torsional angle (28.9°). The DFT calculations also allowed us to determine the strain energy of the nanohoops via the homodesmotic reaction model (Table 1). We used [10]CPP as a benchmark and determined a strain energy of $58.0 \text{ kcal} \cdot \text{mol}^{-1}$, which is in good agreement with a previous calculation ($57.7 \text{ kcal} \cdot \text{mol}^{-1}$).¹⁸ The strain energy of Aza[10]CPP was found to be slightly decreased

($52.9 \text{ kcal} \cdot \text{mol}^{-1}$), which could simply be a result of a lower torsional strain (*vide supra*). Interestingly, *N*-Me-Aza[10]CPP exhibits nearly the same strain energy ($52.4 \text{ kcal} \cdot \text{mol}^{-1}$) as Aza[10]CPP, which we cannot explain with the same simple rationale and may be a result of the cancellation of opposing effects (torsional, steric and internal strain).

We proceeded to study the optical properties of new compounds **9** and **10** in comparison to commercially available [10]CPP by UV-vis absorption and fluorescence spectroscopy (see Figure 1a and Table 1). Since [n]CPPs are centrosymmetric, the HOMO–LUMO transition is Laporte forbidden and the typical absorption band at around 340 nm

Table 1 Selected properties of [10]CPP, Aza[10]CPP and *N*-Me-Aza[10]CPP.

Compound	[10]CPP	Aza[10]CPP	<i>N</i> -Me-Aza[10]CPP
$\lambda(\text{abs})_{\max} [\text{nm}]^a$	340	344	336
$\lambda(\text{em})_{\max} [\text{nm}]^a$	477	471	463
$E(\text{red})_{\text{onset}} [\text{V}]^b$	–	–	–1.54
$K_a [\text{M}^{-1}]^c$	$(2.79 \pm 0.03) \times 10^6$	$(1.1 \pm 0.3) \times 10^7$	$(9.8 \pm 1.6) \times 10^4$
Strain [$\text{kcal} \cdot \text{mol}^{-1}$] ^d	58.0	52.9	52.4
HOMO [eV] ^e	–5.24	–5.27	–5.39
LUMO [eV] ^e	–1.88	–1.96	–2.72

^aMeasured in toluene; ^bTHF, $n\text{Bu}_4\text{PF}_6$, vs. Fc/Fc^+ $V = 100 \text{ mV} \cdot \text{s}^{-1}$; ^cmeasured in toluene; ^dhomodesmotic DFT calculations (B3LYP/6-31 G(d)+D3); ^eDFT calculations (B3LYP/6-31 G(d)+CPCM (acetone/nitrile)).

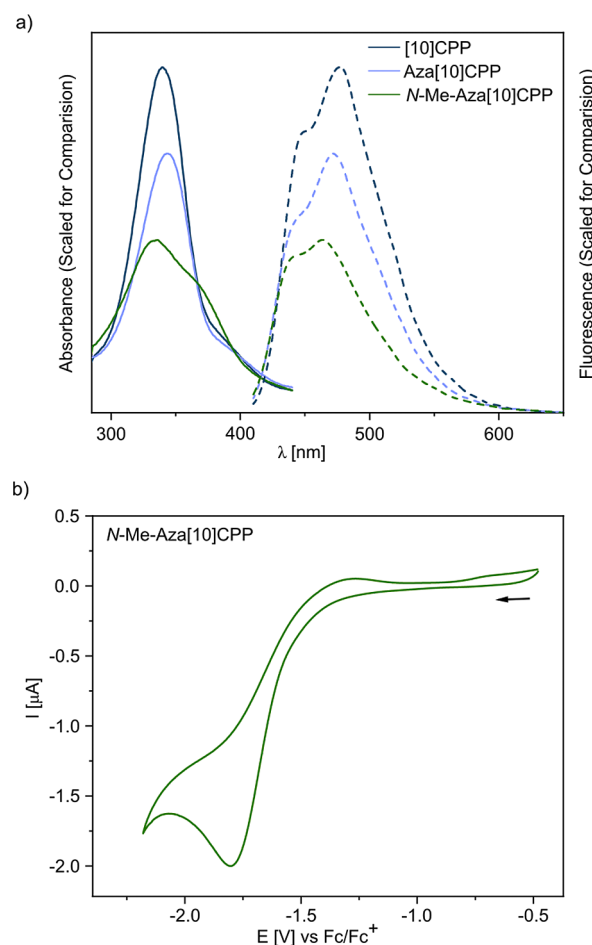


Figure 1 a) Absorbance (solid lines) and fluorescence spectra (dashed lines) of [10]CPP (dark blue): $\lambda(\text{abs})_{\max} = 340 \text{ nm}$ and $\lambda(\text{em})_{\max} = 477 \text{ nm}$; Aza[10]CPP **9** (bright blue): $\lambda(\text{abs})_{\max} = 344 \text{ nm}$ and $\lambda(\text{em})_{\max} = 471 \text{ nm}$; and *N*-Me-Aza[10]CPP **10** (green): $\lambda(\text{abs})_{\max} = 336 \text{ nm}$ and $\lambda(\text{em})_{\max} = 463 \text{ nm}$, in toluene. Spectra are scaled arbitrarily to allow for better comparison. b) Cyclic voltammogram of *N*-Me-Aza[10]CPP **10** in THF using $n\text{Bu}_4\text{PF}_6$ as the electrolyte and Fc/Fc^+ as the internal reference (scan rate: $100 \text{ mV} \cdot \text{s}^{-1}$).

can be assigned to HOMO-2 to LUMO, HOMO-1 to LUMO, HOMO to LUMO+1 and HOMO to LUMO+2.¹⁹ For the pure carbon $[n]$ CPPs the HOMO-1 and HOMO-2 as well as the LUMO+1 and LUMO+2 levels are nearly degenerate. The introduction of a nitrogen atom into the $[8]$ CPP scaffold, as reported previously by Jasti,^{14b,c} broke this degeneracy and led to a slight red-shift of the absorption maximum (Aza $[8]$ CPP and Aza $[6]$ CPP).^{1,2} In the absorbance spectrum of Aza $[10]$ CPP, we also observed a red-shifted maximum (344 nm) compared to $[10]$ CPP (340 nm). However, a small blue-shift was found for *N*-Me-Aza $[10]$ CPP (336 nm), which is not in accordance with Jasti's observations for the smaller methylated nanohoops, where the absorbance maximum was similar to the non-methylated species.^{14b,c} We tentatively attribute these trends to the different observed (solid-state structure) and calculated (minimum DFT structure) torsional angles, which correlate with more or less effective delocalisation of the π -electrons over the whole nanohoop ("radial conjugation").^{3,4b,20}

In contrast to their absorption, the fluorescence of $[n]$ CPPs is size-dependent showing a red-shift and a drop in quantum efficiency by decreasing nanohoop size.^{4a,b} Theoretical studies by Tretiak et al.²¹ showed that fluorescence occurs, according to Kasha's rule, from the lowest energy excited state, which is for larger $[n]$ CPPs ($n \geq 8$) partially planarized, therefore exhibits a different geometry than the ground state and thus becomes allowed. For the previously reported Aza $[8]$ CPP and *N*-Me-Aza $[8]$ CPP, the influence of the electronegative nitrogen also leads to red-shifted emission, which is more pronounced for the methylated species. For the Aza- and *N*-Me-Aza $[10]$ CPPs, we observed the opposite trend with blue-shifting emission maxima from $[10]$ CPP (477 nm) over Aza $[10]$ CPP (471 nm) to *N*-Me-Aza $[10]$ CPP (463 nm). We propose that at least the blue-shift for the *N*-Me-Aza $[10]$ CPP could be explained by its less effective π -conjugation (in analogy to absorption).

For potential applications in organic electronics, the redox properties of a material are of significant interest,²² and it deserves mention that CPPs have found proof-of-principle application in devices.^{1e,13q,15d,e,23} In fact, the ability to access strained nanohoops with low-lying LUMO levels was our major motivation for the synthesis of the compounds reported herein. As such, we were primarily interested in the reduction of the title compounds by means of cyclic voltammetry (THF, $n\text{Bu}_4\text{PF}_6$). Although the chemical reduction of $[n]$ CPPs has been achieved before,²⁴ we were unable to observe the reduction of $[10]$ CPP by cyclic voltammetry, at least within the electrochemical window of the solvent. The same result was observed for Aza $[10]$ CPP, even though we expected a decreased LUMO level based on DFT calculations. However, for *N*-Me-Aza $[10]$ CPP an irreversible reduction wave was observed at an onset potential of -1.54 V vs. the Fc/Fc^+ redox couple (see Figure 1b). Variation of the scan rate did not result in a deviation of the peak shape, therefore, we

conclude that *N*-Me-Aza $[10]$ CPP undergoes an irreversible chemical transformation upon reduction, which is also confirmed by the appearance of new signals in the HRMS analysis after cyclic voltammetry. For *N*-Me-Aza $[6]$ CPP and *N*-Me-Aza $[8]$ CPP, the Jasti group reported irreversible onset reduction potentials of -1.42 and -1.49 V, respectively,^{14b,c} suggesting a lowering of the LUMO with increasing ring size, which is in accordance with the trends reported for pure-carbon $[n]$ CPPs.^{4a}

To better understand the observed photophysical and electrochemical trends, we calculated the frontier orbitals of the studied CPPs using the same DFT method as previously used by Jasti^{14b} (B3LYP/6-31 G(d)+CPCM (acetonitrile), for details see the Supporting Information). The introduction of nitrogen leads to a slight lowering of both the LUMO and the HOMO energy from -1.88 to -1.96 eV and from -5.24 to -5.27 eV, respectively (see Table 1 and Figure S8). Only the methylation leads to a more drastic decrease of the LUMO energy level to -2.72 eV (which is in accordance with the observed reduction in cyclic voltammetry), while the HOMO is again only slightly decreased in energy (-5.39 eV) causing an overall decreased band gap in *N*-Me-Aza $[10]$ CPP. While the calculated frontier orbitals cannot fully explain the observed electronic spectra (e.g. due to symmetry-forbidden transitions), the observed theoretical trends are in good agreement with previous calculations by Jasti et al. for the Aza $[8]$ CPPs.^{14b}

Among the family of $[n]$ CPPs, $[10]$ CPP is of particular interest to supramolecular chemists because of its ability to encapsulate fullerenes with high association constants (K_a).^{13a} The strength of this binding can be determined by fluorescence titrations, during which the fullerene guest is added incrementally to a solution of the $[10]$ CPP host, whose concentration is kept constant throughout the experiment. Thanks to the observed fluorescence quenching and fitting of the corresponding data, a K_a of $(2.79 \pm 0.03) \times 10^6 \cdot \text{M}^{-1}$ (toluene) was determined by Yamago et al.^{13a} for the $[10]$ CPP and C_{60} system. For Aza- and *N*-Me-Aza $[10]$ CPP, we carried out fluorescence titrations in the same way as described above (Figure 2a,b). We found that for Aza $[10]$ CPP the fluorescence quenching is more pronounced (Figure 2c) when compared to *N*-Me-Aza $[10]$ CPP (Figure 2d), which immediately suggests a significantly stronger binding for the former compound. When we fitted the binding isotherms (see Figure 2e) according to a 1 : 1 stoichiometric model, we determined a K_a of $(1.1 \pm 0.3) \times 10^7 \cdot \text{M}^{-1}$ for Aza $[10]$ CPP and a K_a of $(9.8 \pm 1.6) \times 10^4 \cdot \text{M}^{-1}$ for *N*-Me-Aza $[10]$ CPP.²⁵ The two new nanohoops therefore differ by a factor of approximately 100 in their affinity for C_{60} , while the parent nanohoop $[10]$ CPP has intermediate binding strength.

We propose that the relatively weak binding of the methylated nanohoop *N*-Me-Aza $[10]$ CPP may be explained by the steric hindrance due to the methyl group, which sterically desymmetrizes the ring and makes it somewhat less "com-

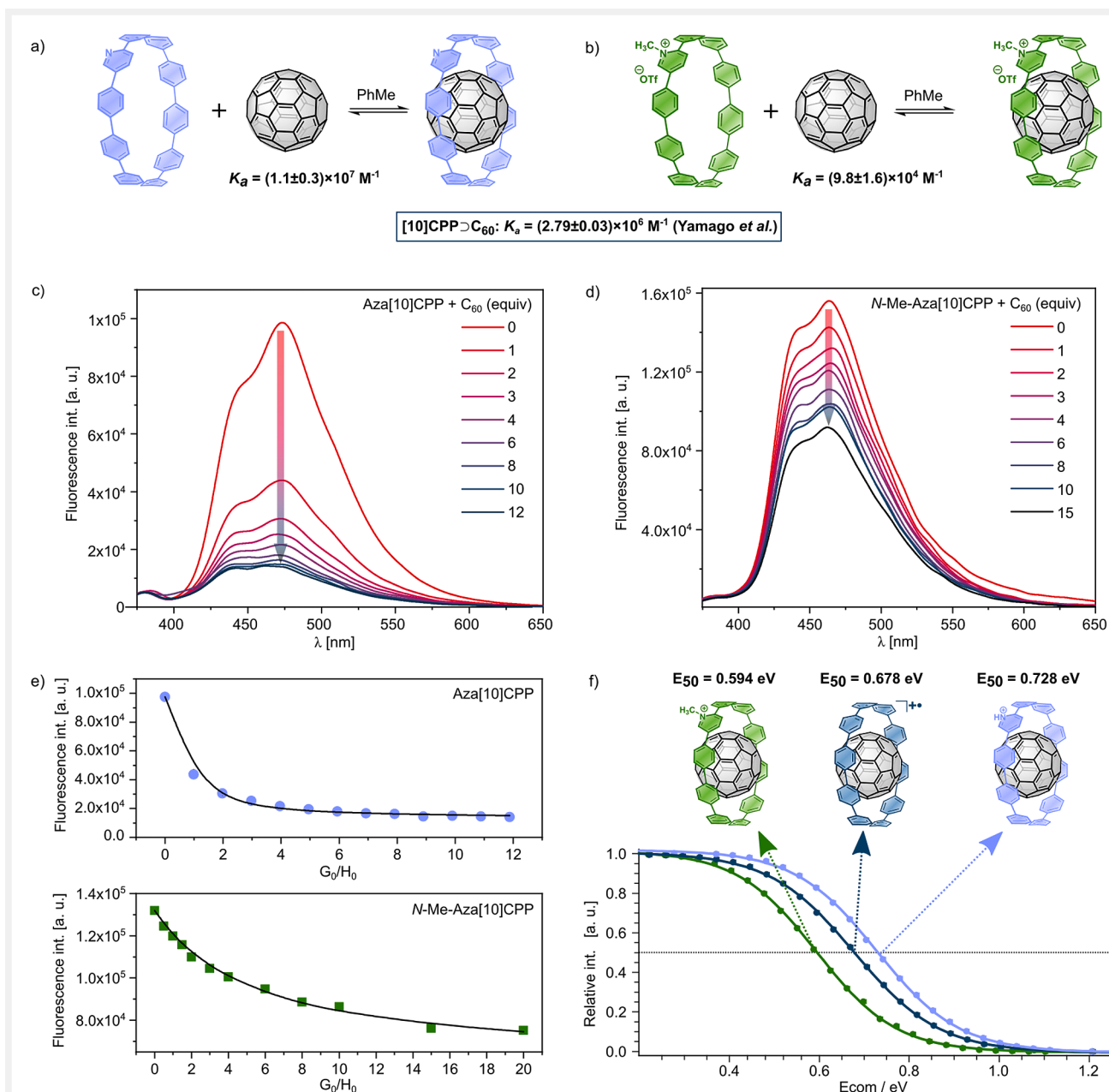


Figure 2 Host-guest equilibria and association constants of C_{60} and a) Aza[10]CPP **9** and b) *N*-Me-Aza[10]CPP **10** compared to [10]CPP^{13a}. Changes in fluorescence spectra upon addition of C_{60} ($\lambda_{exc} = 345$ nm) for c) Aza[10]CPP **9** and d) *N*-Me-Aza[10]CPP **10** in toluene. e) Binding isotherms and fit according to a 1 : 1 model for Aza[10]CPP **9** (blue, at 470 nm) and *N*-Me-Aza[10]CPP **10** (green, at 463 nm). f) Relative abundance of the C_{60} complexes of [10]CPP, Aza[10]CPP **9** and *N*-Me-Aza[10]CPP **10** in ESI-MS/MS with varied collision energy. See the Supporting Information for details.

portable” for the fullerene to occupy the central binding cavity. The significantly higher binding constant of Aza[10]CPP compared with the parent [10]CPP, however, surprised us initially, because we expected that these two compounds would not differ in solvation, shape or strength of dispersion between the host and guest. Nevertheless, the solid-state

structure and the DFT calculations (*vide supra*) suggest that the lower average torsional angles in Aza[10]CPP and the more spherical shape simply make this compound (even) more pre-organized for the binding of C_{60} , which is an effect that also makes suitably sized (partial) nanobelts especially good hosts for C_{60} .^{9t,13d,26} Based on the calculated frontier or-

bital energies of Aza[10]CPP (Table 1), we suggest that this host resembles [10]CPP in the fact that ground-state charge transfer interactions based on the π -systems of host and guest are not at play. However, we cannot rule out a more localized electronic effect based on the interaction of the pyridine lone pair and the π -system of the fullerene (unfortunately, meaningful insights cannot be gained from UV-vis titrations due to extensive signal overlap between C_{60} and Aza[10]CPP).

To obtain further insights into the host-guest chemistry, we decided to study the thermodynamics of the isolated Aza- and *N*-Me-Aza[10]CPP complexes with C_{60} also in the gas phase. In these experiments, the complex is subjected to energy-resolved collisions to induce decomposition while controlling the collision energy. Recording the decline of the charged complex into its fragments as a function of the collision energy in the centre-of-mass frame (see the Supporting Information) results in the so-called survival yield. The collision energy E_{50} , at which 50% of the complex has dissociated into its components, is taken as a relative measure of its stability. The collision experiments (see the Supporting Information) reveal that all three noncovalent complex ions dissociate into a positively charged CPP nanohoop and the neutral C_{60} . The localization of the positive charge on the nanohoops is the result of either protonation or methylation at the nitrogen atom or is caused by oxidation due to a considerably lower ionization energy of the nanohoop compared to C_{60} (see DFT calculations in the Supporting Information). The survival yield curves of the C_{60} complexes with the three nanohoops (Figure 2f) show a clear order of stability. The Aza[10]CPP H^+C_{60} is the most stable complex, followed by [10]CPP $^+C_{60}$ and finally *N*-Me-Aza[10]CPP $^+C_{60}$. The protonated aza-complex, Aza[10]CPP H^+C_{60} , was more abundantly formed in our experiments than the oxidized aza-complex, Aza[10]CPP $^+C_{60}$, and chosen here due to its better signal-to-noise ratio. However, both of these ionic forms of the aza-complex exhibit the same stability. The gas-phase stability of the isolated complexes thus follows the same trend as observed in our solution-based equilibrium studies (*vide supra*).

DFT calculations confirm this stability trend. The fragmentation energies were calculated as the energy differences between the individual nanohoops plus free C_{60} on the one hand and the intact complex on the other hand (see Table S3 in the Supporting Information). The calculations confirm that the fragmentation path of lowest energy requirement would lead in all cases to the charge being located on the nanohoop. Moreover, the Aza[10]CPP H^+C_{60} exhibits a fragmentation energy of 1.82 eV, indicating a stronger binding energy than [10]CPP $^+C_{60}$, for which the fragmentation energy was 1.69 eV.²⁷ The *N*-Me-Aza[10]CPP $^+$ allows for two extreme positions of the methyl group towards the ring, i.e. pointing inwards (“in”) or outwards (“out”). For the “in” conformation of the *N*-Me-Aza

[10]CPP $^+C_{60}$, a fragmentation energy of 1.63 eV was obtained, which would lead to a slightly less stable complex than [10]CPP $^+C_{60}$, as confirmed by the collision experiments. The “out” conformation shows with fragmentation energy of 1.81 eV, a similar stability to the Aza[10]CPP H^+C_{60} complex. It is well established that in solution the phenyl groups of a CPP ring show a considerable “fluttering” within their complexes even at relatively low temperatures.^{9m,13a} We assume here a similar fluctuation in the gas phase between “in” and “out” like positions of the methyl group leading to the overall weakest bonding between the nanohoop and fullerene sphere, as observed in the collision experiments.

CPPs have emerged as suitable electron donors in conjunction with fullerenes,^{13m} and as supramolecular mediators of charge transfer between porphyrins and fullerenes.^{8f} To compare the influence of Aza[10]CPP and *N*-Me-Aza[10]CPP relative to [10]CPP, we turned to time-resolved transient absorption spectroscopy (TAS) on the fs- and ns-timescale in the presence of electron-accepting C_{60} . To probe different solvent polarities, we prepared mixtures of the different CPPs and C_{60} in toluene and THF at concentrations of 5×10^{-5} M. Considering the low solubility of C_{60} in THF, all mixtures were first prepared in toluene with a 1 : 1 molar ratio of the CPPs and C_{60} . Subsequently, toluene was evaporated and the residue dissolved in THF. Absorption spectroscopy confirmed the presence of the CPPs as well as C_{60} . 387 nm was selected as the excitation wavelength for the time-resolved measurements, as it predominantly excites the CPPs.²⁸ Initially, the three different CPPs were probed in the absence of C_{60} . In each case, deconvolution of the spectra via global target analysis afforded three main species. The first species on the fs-timescale is assigned to a hot singlet excited state of the CPP with lifetimes ranging from 1 to 132 ps. In parallel to its decay, a second species is formed, whose lifetime was derived from ns-TAS as its lifetime exceeded the fs-timeframe.

It is assigned to a relaxed singlet excited state of the corresponding CPP.²⁹ Lifetimes of the second species range from 5.7 ns for [10]CPP to 1.4 and 2.5 ns for Aza[10]CPP and *N*-Me-Aza[10]CPP, respectively. Eventually, a third species evolves with a lifetime of 0.6 μ s for [10]CPP, which is assigned to its triplet excited state.³⁰ Overall, the species-associated spectra (SAS) show very similar features for [10]CPP and Aza[10]CPP. To this end, the first and second species reveal features at 490, 670, 724 and 893 nm, while the third species displays a broad band around 665 nm. In contrast, all SAS of *N*-Me-Aza[10]CPP show a very broad absorption across the entire visible range as well as a feature at 820 nm for the singlet excited states.

Addition of C_{60} to the three different CPPs introduces considerable changes in the 3D fs- and ns-TAS heat maps for the resulting CPP $^+C_{60}$ complexes. Deconvolution via global target analysis prompted also to the existence of

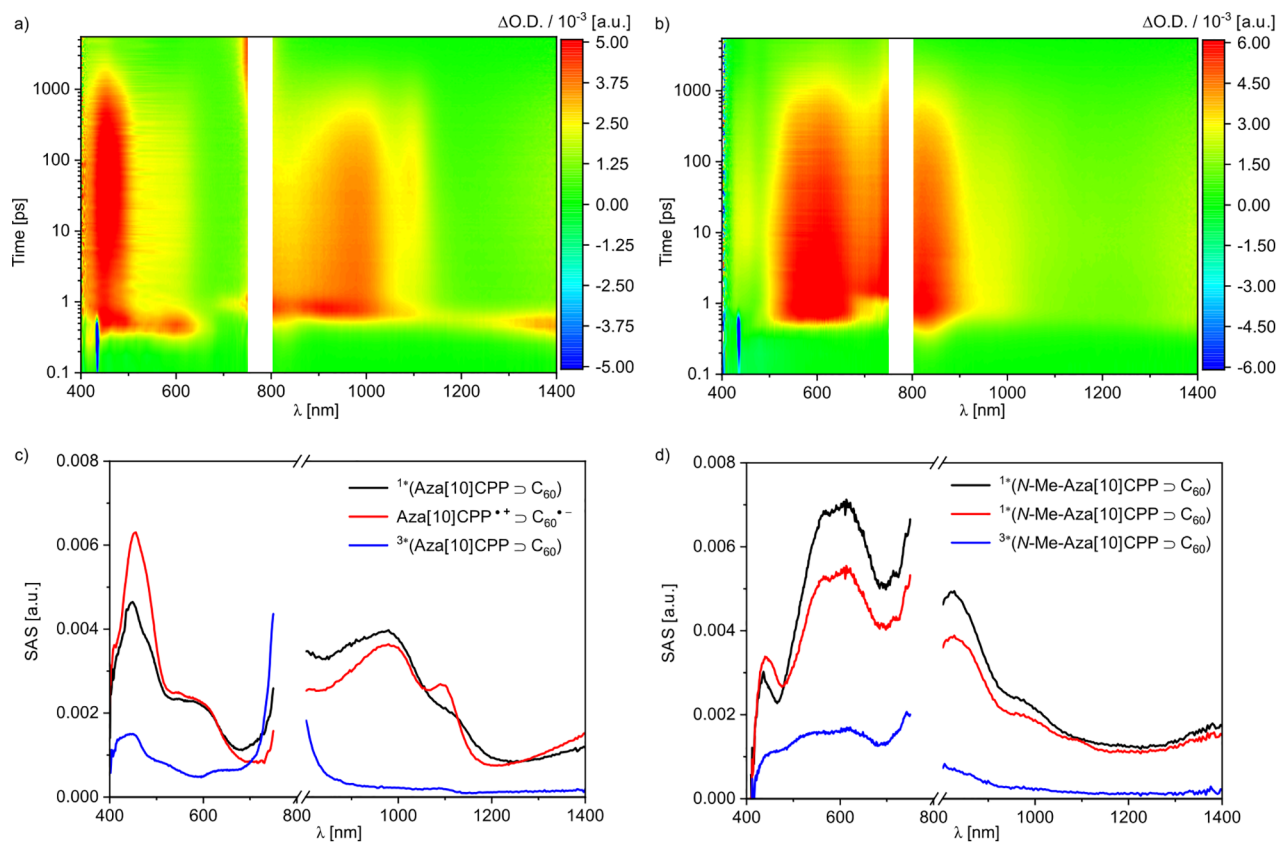


Figure 3 Differential absorption spectra of a) Aza[10]CPP **9** and b) *N*-Me-Aza[10]CPP **10** with C₆₀ (5×10^{-5} M, 1:1) obtained by fs-TAS at time delays between 0.1 and 5500 ps after laser excitation at 387 nm measured in THF. Deconvoluted SAS obtained via global target analysis following a sequential model (black–red–blue) of c) Aza[10]CPP **9** and d) *N*-Me-aza[10]CPP **10**.

three species (Figure 3a). Those features which were seen for the singlet excited states of [10]CPP and Aza[10]CPP were missing. Instead, 460 and 980 nm signatures characterize the first species. Its lifetime is around 8 ps and in light of the appreciable ground-state interactions, we postulate the direct charge-transfer population by photoexcitation. Following its decay, an additional feature at 1090 nm grows in as the second species evolves, which is a known fingerprint of the one-electron-reduced form of C₆₀ (Figure 3c).^{31,32} Apart from that, the 460 nm marker represents the one-electron-oxidized form of the CPPs. Taken the aforementioned into concert, we confirmed electron transfer to C₆₀ and, in turn, formation of the charge-separated states [10]CPP^{•+}⊃C₆₀^{•-} as well as Aza[10]CPP^{•+}⊃C₆₀^{•-} as the second species.^{13m}

The lifetimes are 1.6 and 1.4 ns, respectively. ns-TAS spectra are dominated by a signal at 750 nm and lifetimes of 25 and 24 μs. This speaks for a charge recombination, which yields the triplet excited state.³¹

In contrast, adding C₆₀ to *N*-Me-Aza[10]CPP leads to no significant changes in the 3D heat maps and no detection of the fingerprint of the one-electron-reduced form of C₆₀ (Figure 3b,d), it is only on the longer ns-timescale, where the C₆₀ triplet excited state is quenched compared to the other two CPPs. This finding is not simply due to the lower association constant (compared to [10]CPP and Aza[10]CPP), because approx. 65% of the host–guest complex should be associated under the conditions of the experiment. We suggest that, in addition to the low LUMO level (see also Table 1), the positive charge density at the nanohoop in *N*-Me-Aza[10]CPP might prohibit any electron transfer to C₆₀.

Conclusions

We were able to employ a synthesis protocol developed by Jasti to prepare the previously unknown nitrogen-doped nanohoops Aza[10]CPP and *N*-Me-Aza[10]CPP. A comparative study of fundamental properties of the three related

[10]CPP nanohoops revealed the following insights: (i) the main absorption and fluorescence bands show only slight shifts that are largely in agreement with results observed for the smaller nitrogen-doped CPPs.^{14b,c} (ii) Aza[10]CPP binds C₆₀ about 20 times more strongly than [10]CPP, while *N*-Me-Aza[10]CPP binds C₆₀ with a 10-fold lower affinity than [10]CPP. Because these trends were also observed in the gas phase, we propose that the high C₆₀ affinity of Aza[10]CPP is a consequence of lower torsional angles between phenylenes, which is corroborated by observations we made in the solid state and by DFT calculations. The decreased C₆₀ affinity of the charged *N*-Me-Aza[10]CPP is most likely a steric rather than an electronic effect. (iii) Ultrafast transient absorption studies revealed that photo-induced electron transfer occurs in [10]CPP>C₆₀ as well as Aza[10]CPP>C₆₀ in THF, where both CPPs follow a similar deactivation pattern following laser excitation. In stark contrast, no electron transfer was seen in *N*-Me-Aza[10]CPP>C₆₀. We believe that the results of this study at the interface of supramolecular and materials chemistry will prove useful for researchers seeking to create self-assembled functional materials.^{15d,33}

Experimental Section

All commercially available chemicals were purchased from Sigma Aldrich, TCI Germany, VWR International, Fischer Scientific, Carl Roth GmbH & Co., Acros Organics or Alfa Aesar. All of them were used without further purification. Anhydrous solvents were dried prior to use on an MBraun SPS-800 system.

For details on instrumentation and detailed methods, please refer to the Supporting Information.

Synthetic Procedures

Synthesis of compound 8: Under N₂, **6** (200 mg, 0.20 mmol, 1.0 equiv), **7** (93.0 mg, 0.20 mmol, 1.0 equiv), NaHCO₃ (168 mg, 2.00 mmol, 10 equiv) and *n*-Bu₄NBr (13.0 mg, 0.040 mmol, 0.2 equiv) were added to a pressure flask and dissolved in a mixture of degassed toluene (45 mL), methanol (5 mL) and water (2.5 mL). The mixture was degassed for 10 min using a N₂ stream, Pd(PPh₃)₄ (23.0 mg, 0.020 mmol, 0.1 equiv) was added and the mixture was heated to 90 °C for 18 h. The organic solvents were removed under reduced pressure, brine (50 mL) was added and the mixture was extracted with CH₂Cl₂ (2 × 50 mL). The combined organic layers were dried over MgSO₄ and concentrated under reduced pressure. The crude product was purified by column chromatography (CH₂Cl₂/EtOAc 5:1 → 3:1) to remove less polar side-products. The fraction-containing product and some minor impurities were used without further purification for the next step.

Synthesis of Aza[10]CPP 9: Under N₂, naphthalene (641 mg, 5.00 mmol, 1.0 equiv) was dissolved in anhydrous THF (10 mL). Small pieces of sodium metal (171 mg, 7.50 mmol, 1.5 equiv) was added to the solution, which was stirred for 16 h at room temperature yielding sodium naphthalenide as a dark green solution. Under N₂, **8** (28.0 mg, 0.028 mmol, 1.0 equiv) was dissolved in anhydrous THF (10 mL) and cooled down to −78 °C. The freshly prepared solution of sodium naphthalenide (1.32 mL, 0.5 M, 0.653 mmol, 24.0 equiv) was added dropwise, yielding a dark violet solution which was stirred at −78 °C for further 90 min. The reaction was quenched by adding a solution of iodine in THF. An aqueous solution of Na₂S₂O₃ was added and the reaction was extracted with CH₂Cl₂ (2 × 50 mL) and the combined organic layers were dried over MgSO₄ and concentrated under reduced pressure. The crude product was purified by column chromatography (CH₂Cl₂/PE 2:1 → DCM) to yield **9** as a yellow solid (13.0 mg, 0.017 mmol, 9% over two steps).

¹H NMR (CDCl₃, 500 MHz): δ = 8.85 (d, ⁴J = 2.3 Hz, 1 H, H_C), 8.03 (d, ³J = 8.7 Hz, 2 H, Ph-H), 7.98 (dd, ³J = 8.6, ⁴J = 2.3 Hz, 1 H, H_B), 7.73 (d, ³J = 8.6 Hz, 1 H, H_A), 7.64 (d, ³J = 8.8 Hz, 2 H), 7.60–7.49 (m, 32H, Ph-H) ppm.

¹³C NMR (CDCl₃, 101 MHz): δ = 154.8, 147.5, 139.9, 139.1, 138.7, 138.5, 138.5, 138.4, 138.4, 138.3, 138.3, 138.2, 138.2, 137.4, 135.3, 133.3, 132.7, 131.7, 128.8, 128.0, 127.9, 127.7, 127.6, 127.6, 127.5, 127.5, 127.4, 127.4, 119.5, 115.5 ppm.

HRMS (MALDI): *m/z* calcd for C₅₉H₃₉N: 761.3083, found: 761.3078 [M]⁺.

Synthesis of *N*-Me-Aza[10]CPP 10: Under N₂, Aza[10]CPP **9** (3.5 mg, 4.6 μmol, 1.0 equiv) was dissolved in anhydrous CH₂Cl₂ (3 mL). Methyl triflate (2.5 μL, 23 μmol, 5 equiv) was added dropwise. The color of the reaction solution changed from a bright yellow to a darker yellow. The reaction was stirred for 20 h at room temperature and quenched by addition of aqueous NH₄Cl solution. The aqueous phase was separated, extracted with CH₂Cl₂ (2 × 20 mL) and the combined organic layers were dried over Mg₂SO₄. The solvent was removed under reduced pressure and the crude product was purified by column chromatography (CH₂Cl₂ → 5% MeOH in CH₂Cl₂) to yield **10** as a yellow solid (3.8 mg, 4.1 μmol, 89%).

¹H NMR (CDCl₃, 400 MHz): δ = 9.63 (d, ⁴J = 1.9 Hz, 1 H, H_C), 8.06 (dd, ³J = 8.7, ⁴J = 1.8 Hz, 1 H, H_B), 7.84 (d, ³J = 8.5 Hz, 2 H, Ph-H), 7.73 (d, ³J = 8.6 Hz, 2 H), 7.69–7.50 (m, 32 H, Ph-H), 7.45 (d, ³J = 8.6 Hz, 1 H, H_A), 4.81 (s, 3 H, CH₃) ppm.

¹³C NMR (101 MHz, CDCl₃): δ = 152.5, 145.1, 144.6, 141.7, 141.7, 139.8, 139.5, 139.0, 138.5, 138.4, 138.4, 138.3, 138.2, 138.2, 138.0, 137.4, 137.1, 137.0, 130.9, 130.7, 129.7, 129.7, 129.2, 129.1, 128.3, 127.8, 127.7, 127.6, 127.6, 127.5, 48.3 ppm.

¹⁹F NMR (376 MHz, CDCl₃) δ = −78.23 ppm.

HRMS (MALDI): *m/z* = calcd. for C₆₀H₆₂N: 776.3317, found: 776.3322 [M]⁺.

Further synthetic procedures are described in the Supporting Information.

Funding Information

The authors acknowledge financial support by the Deutsche Forschungsgemeinschaft (DFG) Projektnummer 182 849 149-SFB953 “Synthetic Carbon Allotropes” (projects A7, B10, C2, Z1) and infrastructure provided by the state of Baden-Württemberg through bwHPC and the DFG through grant no. INST 40/575–1 FUGG (JUSTUS 2 cluster). M.F. acknowledges financial support by the Hanns-Seidel-Stiftung.

Acknowledgment

We would like to thank Oleg Borodin for helpful advice on spectrophotometric host–guest titrations.

Supporting Information

Supporting Information for this article is available online at <https://doi.org/10.1055/a-1814-7686>.

Conflict of Interest

The authors declare no conflict of interest.

References

- (1) (a) Tran-Van, A.-F.; Wegner, H. A. *Beilstein J. Nanotechnol.* **2014**, *5*, 1320. (b) Darzi, E. R.; Jasti, R. *Chem. Soc. Rev.* **2015**, *44*, 6401. (c) Lewis, S. E. *Chem. Soc. Rev.* **2015**, *44*, 2221. (d) Segawa, Y.; Yagi, A.; Matsui, K.; Itami, K. *Angew. Chem. Int. Ed.* **2016**, *55*, 5136. (e) Wu, D.; Cheng, W.; Ban, X.; Xia, J. *Asian J. Org. Chem.* **2018**, *7*, 2161. (f) Yamago, S.; Kayahara, E. *J. Synth. Org. Chem. Jpn.* **2019**, *77*, 1147. (g) Griwatz, J. H.; Wegner, H. A. *Org. Mater.* **2020**, *02*, 306. (h) Li, Y.; Kono, H.; Maekawa, T.; Segawa, Y.; Yagi, A.; Itami, K. *Acc. Mater. Res.* **2021**, *2*, 681.
- (2) (a) Cheung, K. Y.; Segawa, Y.; Itami, K. *Chem. Eur. J.* **2020**, *26*, 14791. (b) Chen, H.; Miao, Q. *J. Phys. Org. Chem.* **2020**, *33*, e4152. (c) Guo, Q.-H.; Qiu, Y.; Wang, M.-X.; Stoddart, F. J. *Nat. Chem.* **2021**, *13*, 402.
- (3) Jasti, R.; Bhattacharjee, J.; Neaton, J. B.; Bertozzi, C. R. *J. Am. Chem. Soc.* **2008**, *130*, 17646.
- (4) (a) Yamago, S.; Kayahara, E.; Iwamoto, T. *Chem. Rec.* **2014**, *14*, 84. (b) Golder, M. R.; Jasti, R. *Acc. Chem. Res.* **2015**, *48*, 557.
- (5) (a) Xu, Y.; Delius, M. *Angew. Chem. Int. Ed.* **2020**, *59*, 559. (b) Lu, D.; Huang, Q.; Wang, S.; Wang, J.; Huang, P.; Du, P. *Front. Chem.* **2019**, *7*, 668. (c) Beil, S. B.; von Delius, M. *Org. Mater.* **2021**, *03*, 146. (d) Yang, Y.; Juriček, M. *ChemPlusChem.* **2021**, in press; DOI: doi:10.1002/cplu.202100468.
- (6) Wang, J.; Zhang, X.; Jia, H.; Wang, S.; Du, P. *Acc. Chem. Res.* **2021**, *54*, 4178.
- (7) Hermann, M.; Wassy, D.; Esser, B. *Angew. Chem. Int. Ed.* **2021**, *60*, 15743.
- (8) (a) Xia, J.; Golder, M. R.; Foster, M. E.; Wong, B. M.; Jasti, R. *J. Am. Chem. Soc.* **2012**, *134*, 19709. (b) Ishii, Y.; Matsuura, S.; Segawa, Y.; Itami, K. *Org. Lett.* **2014**, *16*, 2174. (c) Kayahara, E.; Qu, R.; Yamago, S. *Angew. Chem. Int. Ed.* **2017**, *56*, 10428. (d) Leonhardt, E. J.; Van Raden, J. M.; Miller, D.; Zakharov, L. N.; Alemán, B.; Jasti, R. *Nano Lett.* **2018**, *18*, 7991. (e) Hashimoto, S.; Kayahara, E.; Mizuhata, Y.; Tokitoh, N.; Takeuchi, K.; Ozawa, F.; Yamago, S. *Org. Lett.* **2018**, *20*, 5973. (f) Xu, Y.; Wang, B.; Kaur, R.; Minameyer, M. B.; Bothe, M.; Drewello, T.; Guld, D. M.; von Delius, M. *Angew. Chem. Int. Ed.* **2018**, *57*, 11549. (g) Van Raden, J. M.; Leonhardt, E. J.; Zakharov, L. N.; Pérez-Guardiola, A.; Pérez-Jiménez, A. J.; Marshall, C. R.; Brozek, C. K.; Sancho-García, J. C.; Jasti, R. *J. Org. Chem.* **2020**, *85*, 129. (h) Itami, K.; Shudo, H.; Kuwayama, M.; Shimasaki, M.; Nishihara, T.; Takeda, Y.; Kuwabara, T.; Yagi, A.; Segawa, Y. **2021**, *ChemRxiv*, DOI: doi:10.33774/chemrxiv-2021-7kd63.
- (9) (a) Nishiuchi, T.; Feng, X.; Enkelmann, V.; Wagner, M.; Müllen, K. *Chem. Eur. J.* **2012**, *18*, 16621. (b) Yagi, A.; Segawa, Y.; Itami, K. *J. Am. Chem. Soc.* **2012**, *134*, 2962. (c) Batson, J. M.; Swager, T. M. *Synlett* **2013**, *24*, 2545. (d) Tran-Van, A.-F.; Huxol, E.; Basler, J. M.; Neuburger, M.; Adjizian, J.-J.; Ewels, C. P.; Wegner, H. A. *Org. Lett.* **2014**, *16*, 1594. (e) Iwamoto, T.; Kayahara, E.; Yasuda, N.; Suzuki, T.; Yamago, S. *Angew. Chem. Int. Ed.* **2014**, *53*, 6430. (f) Kubota, N.; Segawa, Y.; Itami, K. *J. Am. Chem. Soc.* **2015**, *137*, 1356. (g) Miyauchi, Y.; Johmoto, K.; Yasuda, N.; Uekusa, H.; Fujii, S.; Kiguchi, M.; Ito, H.; Itami, K.; Tanaka, K. *Chem. Eur. J.* **2015**, *21*, 18900. (h) Sarkar, P.; Sato, S.; Kamata, S.; Matsuno, T.; Isobe, H. *Chem. Lett.* **2015**, *44*, 1581. (i) Kuroda, Y.; Sakamoto, Y.; Suzuki, T.; Kayahara, E.; Yamago, S. *J. Org. Chem.* **2016**, *81*, 3356. (j) Ike-moto, K.; Fujita, M.; Too, P. C.; Tnay, Y. L.; Sato, S.; Chiba, S.; Isobe, H. *Chem. Lett.* **2016**, *45*, 658. (k) Li, P.; Wong, B. M.; Zakharov, L. N.; Jasti, R. *Org. Lett.* **2016**, *18*, 1574. (l) Lu, D.; Wu, H.; Dai, Y.; Shi, H.; Shao, X.; Yang, S.; Yang, J.; Du, P. *Chem. Commun.* **2016**, *52*, 7164. (m) Della Sala, P.; Talotta, C.; Caruso, T.; De Rosa, M.; Soriente, A.; Neri, P.; Gaeta, C. *J. Org. Chem.* **2017**, *82*, 9885. (n) Nishigaki, S.; Fukui, M.; Sugiyama, H.; Uekusa, H.; Kawachi, S.; Shibata, Y.; Tanaka, K. *Chem. Eur. J.* **2017**, *23*, 7227. (o) Lu, D.; Zhuang, G.; Jia, H.; Wang, J.; Huang, Q.; Cui, S.; Du, P. *Org. Chem. Front.* **2018**, *5*, 1446. (p) Povie, G.; Segawa, Y.; Nishihara, T.; Miyauchi, Y.; Itami, K. *J. Am. Chem. Soc.* **2018**, *140*, 10054. (q) Jia, H.; Gao, Y.; Huang, Q.; Cui, S.; Du, P. *Chem. Commun.* **2018**, *54*, 988. (r) White, B. M.; Zhao, Y.; Kawashima, T. E.; Branchaud, B. P.; Pluth, M. D.; Jasti, R. *ACS Cent. Sci.* **2018**, *4*, 1173. (s) Della Sala, P.; Talotta, C.; De Rosa, M.; Soriente, A.; Geremia, S.; Hickey, N.; Neri, P.; Gaeta, C. *J. Org. Chem.* **2019**, *84*, 9489. (t) Huang, Q.; Zhuang, G.; Jia, H.; Qian, M.; Cui, S.; Yang, S.; Du, P. *Angew. Chem. Int. Ed.* **2019**, *58*, 6244. (u) Huang, Q.; Zhuang, G.; Zhang, M.; Wang, J.; Wang, S.; Wu, Y.; Yang, S.; Du, P. *J. Am. Chem. Soc.* **2019**, *141*, 18938. (v) Nishigaki, S.; Shibata, Y.; Nakajima, A.; Okajima, H.; Masumoto, Y.; Osawa, T.; Muranaka, A.; Sugiyama, H.; Horikawa, A.; Uekusa, H.; Koshino, H.; Uchiyama, M.; Sakamoto, A.; Tanaka, K. *J. Am. Chem. Soc.* **2019**, *141*, 14955. (w) Lovell, T. C.; Garrison, Z. R.; Jasti, R. *Angew. Chem. Int. Ed.* **2020**, *59*, 14363. (x) Peters, G. M.; Grover, G.; Maust, R. L.; Colwell, C. E.; Bates, H.; Edgell, W. A.; Jasti, R.; Kertesz, M.; Tovar, J. D. *J. Am. Chem. Soc.* **2020**, *142*, 2293. (y) Kayahara, E.; Nakano, M.; Sun, L.; Ishida, K.; Yamago, S. *Chem. Asian J.* **2020**, *15*, 2451. (z) Huang, Q.; Wu, Y.; Zhou, Y.; Liu, H.; Wang, J.; Wang, S.; Du, P. *Synthesis* **2020**, *52*, 2535. (aa) Grabicki, N.; Nguyen, K. T. D.; Weidner, S.; Dumele, O. *Angew. Chem. Int. Ed.*

- 2021**, 60, 14909. (ab) Volkmann, J.; Kohrs, D.; Bernt, F.; Wegner, H. A. *Eur. J. Org. Chem.* **2021**, in press; DOI: doi:10.1002/ejoc.202101357. (ac) Zhang, X.; Shi, H.; Zhuang, G.; Wang, S.; Wang, J.; Yang, S.; Shao, X.; Du, P. *Angew. Chem. Int. Ed.* **2021**, 60, 17368. (ad) Wang, S.; Li, X.; Zhuang, G.; Chen, M.; Huang, P.; Yang, S.; Du, P. *Chem. Commun.* **2021**, 57, 9104. (ae) Li, K.; Xu, Z.; Deng, H.; Zhou, Z.; Dang, Y.; Sun, Z. *Angew. Chem. Int. Ed.* **2021**, 60, 7649. (af) Nishigaki, S.; Shibata, Y.; Nakajima, A.; Okajima, H.; Masumoto, Y.; Osawa, T.; Muranaka, A.; Sugiyama, H.; Hori-kawa, A.; Uekusa, H.; Koshino, H.; Uchiyama, M.; Sakamoto, A.; Tanaka, K. *J. Am. Chem. Soc.* **2019**, 141, 14955.
- (10) Segawa, Y.; Kuwayama, M.; Hijikata, Y.; Fushimi, M.; Nishihara, T.; Pirillo, J.; Shirasaki, J.; Kubota, N.; Itami, K. *Science* **2019**, 365, 272.
- (11) (a) Matsui, K.; Segawa, Y.; Namikawa, T.; Kamada, K.; Itami, K. *Chem. Sci.* **2012**, 4, 84. (b) Kayahara, E.; Iwamoto, T.; Takaya, H.; Suzuki, T.; Fujitsuka, M.; Majima, T.; Yasuda, N.; Matsuyama, N.; Seki, S.; Yamago, S. *Nat. Commun.* **2013**, 4, 2694. (c) Matsui, K.; Segawa, Y.; Itami, K. *J. Am. Chem. Soc.* **2014**, 136, 16452.
- (12) (a) Huang, Z.-A.; Chen, C.; Yang, X.-D.; Fan, X.-B.; Zhou, W.; Tung, C.-H.; Wu, L.-Z.; Cong, H. *J. Am. Chem. Soc.* **2016**, 138, 11144. (b) Senthilkumar, K.; Kondratowicz, M.; Lis, T.; Chmielewski, P. J.; Cybińska, J.; Zafra, J. L.; Casado, J.; Vives, T.; Crassous, J.; Favereau, L.; Stępień, M. *J. Am. Chem. Soc.* **2019**, 141, 7421. (c) Xu, W.; Yang, X.-D.; Fan, X.-B.; Wang, X.; Tung, C.-H.; Wu, L.-Z.; Cong, H. *Angew. Chem. Int. Ed.* **2019**, 58, 3943. (d) Schaub, T. A.; Prantl, E. A.; Kohn, J.; Bursch, M.; Marshall, C. R.; Leonhardt, E. J.; Lovell, T. C.; Zakharov, L. N.; Brozek, C. K.; Waldivogel, S. R.; Grimme, S.; Jasti, R. *J. Am. Chem. Soc.* **2020**, 142, 8763. (e) Cong, H. *Chem. Lett.* **2021**, 50, 819. (f) Yang, Y.; Blacque, O.; Sato, S.; Juriček, M. *Angew. Chem. Int. Ed.* **2021**, 60, 13529.
- (13) (a) Iwamoto, T.; Watanabe, Y.; Sadahiro, T.; Haino, T.; Yamago, S. *Angew. Chem. Int. Ed.* **2011**, 50, 8342. (b) Xia, J.; Bacon, J. W.; Jasti, R. *Chem. Sci.* **2012**, 3, 3018. (c) Iwamoto, T.; Watanabe, Y.; Takaya, H.; Haino, T.; Yasuda, N.; Yamago, S. *Chem. Eur. J.* **2013**, 19, 14061. (d) Isobe, H.; Hitosugi, S.; Yamasaki, T.; Iizuka, R. *Chem. Sci.* **2013**, 4, 1293. (e) Sato, S.; Yamasaki, T.; Isobe, H. *PNAS* **2014**, 111, 8374. (f) Matsuno, T.; Sato, S.; Iizuka, R.; Isobe, H. *Chem. Sci.* **2015**, 6, 909. (g) Isobe, H.; Nakamura, K.; Hitosugi, S.; Sato, S.; Tokoyama, H.; Yamakado, H.; Ohno, K.; Kono, H. *Chem. Sci.* **2015**, 6, 2746. (h) Matsuno, T.; Sato, S.; Yokoyama, A.; Kamata, S.; Isobe, H. *Angew. Chem. Int. Ed.* **2016**, 55, 15339. (i) Matsuno, T.; Kamata, S.; Sato, S.; Yokoyama, A.; Sarkar, P.; Isobe, H. *Angew. Chem. Int. Ed.* **2017**, 56, 15020. (j) Matsuno, T.; Nakai, Y.; Sato, S.; Maniwa, Y.; Isobe, H. *Nat. Commun.* **2018**, 9, 1907. (k) Sun, Z.; Mio, T.; Okada, P.; Matsuno, T.; Sato, S.; Kono, H.; Isobe, H. *Angew. Chem. Int. Ed.* **2019**, 58, 2040. (l) Rio, J.; Beeck, S.; Rotas, G.; Ahles, S.; Jacquemin, D.; Tagmatarchis, N.; Ewels, C.; Wegner, H. A. *Angew. Chem. Int. Ed.* **2018**, 57, 6930. (m) Xu, Y.; Kaur, R.; Wang, B.; Minameyer, M. B.; Gsänger, B.; Meyer, B.; Drewello, T.; Guldi, D. M.; von Delius, M. *J. Am. Chem. Soc.* **2018**, 140, 13413. (n) Xu, Y.; Gsänger, S.; Minameyer, M. B.; Imaz, I.; Maspoch, D.; Shyshov, O.; Schwer, F.; Ribas, X.; Drewello, T.; Meyer, B.; von Delius, M. *J. Am. Chem. Soc.* **2019**, 141, 18500. (o) Cui, S.; Huang, Q.; Wang, J.; Jia, H.; Huang, P.; Wang, S.; Du, P. *Org. Lett.* **2019**, 21, 5917. (p) Ubasart, E.; Borodin, O.; Fuertes-Espinosa, C.; Xu, Y.; García-Simón, C.; Gómez, L.; Juanhuix, J.; Gándara, F.; Imaz, I.; Maspoch, D.; von Delius, M.; Ribas, X. *Nat. Chem.* **2021**, 13, 420. (q) Wang, S.; Li, X.; Zhang, X.; Huang, P.; Fang, P.; Wang, J.; Yang, S.; Wu, K.; Du, P. *Chem. Sci.* **2021**, 12, 10506. (r) Yang, Y.; Huangfu, S.; Sato, S.; Juriček, M. *Org. Lett.* **2021**, 23, 7943.
- (14) (a) Matsui, K.; Segawa, Y.; Itami, K. *Org. Lett.* **2012**, 14, 1888. (b) Darzi, E. R.; Hirst, E. S.; Weber, C. D.; Zakharov, L. N.; Loneragan, M. C.; Jasti, R. *ACS Cent. Sci.* **2015**, 1, 335. (c) Van Raden, J. M.; Darzi, E. R.; Zakharov, L. N.; Jasti, R. *Org. Biomol. Chem.* **2016**, 14, 5721. (d) Van Raden, J. M.; Louie, S.; Zakharov, L. N.; Jasti, R. *J. Am. Chem. Soc.* **2017**, 139, 2936. (e) Chen, M.; Unikela, K. S.; Ramalakshmi, R.; Li, B.; Darrigan, C.; Chrostowska, A.; Liu, S.-Y. *Angew. Chem. Int. Ed.* **2021**, 60, 1556.
- (15) (a) García, J. C.; Moral, M.; Pérez-Jiménez, A. J. *J. Phys. Chem. C* **2016**, 120, 9104. (b) Kayahara, E.; Sun, L.; Onishi, H.; Suzuki, K.; Fukushima, T.; Sawada, A.; Kaji, H.; Yamago, S. *J. Am. Chem. Soc.* **2017**, 139, 18480. (c) Lin, J. B.; Darzi, E. R.; Jasti, R.; Yavuz, I.; Houk, K. N. *J. Am. Chem. Soc.* **2019**, 141, 952. (d) Leonhardt, E. J.; Jasti, R. *Nat. Rev. Chem.* **2019**, 3, 672. (e) Lv, Y.; Link, J.; Song, K.; Song, X.; Zang, H.; Zang, Y.; Zhu, D. *Sci. Adv.* **2021**, in press; DOI: doi:10.1126/sciadv.abk3095.
- (16) Kayahara, E.; Sakamoto, Y.; Suzuki, T.; Yamago, S. *Org. Lett.* **2012**, 14, 3284.
- (17) Bachrach, S. M.; Stück, D. *J. Org. Chem.* **2010**, 75, 6595.
- (18) Segawa, Y.; Omachi, H.; Itami, K. *Org. Lett.* **2010**, 12, 2262.
- (19) Iwamoto, T.; Watanabe, Y.; Sakamoto, Y.; Suzuki, T.; Yamago, S. *J. Am. Chem. Soc.* **2011**, 133, 8354.
- (20) Scott, L. T. *Angew. Chem. Int. Ed.* **2003**, 42, 4133.
- (21) Adamska, L.; Nayyar, I.; Chen, H.; Swan, A. K.; Oldani, N.; Fernandez-Albertini, S.; Golder, M. R.; Jasti, R.; Doorn, S. K.; Tretiak, S. *Nano Lett.* **2014**, 14, 6539.
- (22) (a) Segura, J. L.; Martín, N.; Guldi, D. M. *Chem. Soc. Rev.* **2005**, 34, 31. (b) Yang, Z.; Mao, Z.; Xie, Z.; Zhang, Y.; Liu, S.; Zhao, J.; Xu, J.; Chi, Z.; Aldred, M. P. *Chem. Soc. Rev.* **2017**, 46, 915. (c) Zhang, L.; Qian, Y.; Feng, R.; Ding, Y.; Zhang, Y.; Guo, X.; Wang, W.; Yu, G. *Nat. Commun.* **2020**, 11, 3843.
- (23) Tang, Y.; Li, J.; Du, P.; Zhang, H.; Zheng, C.; Lin, H.; Du, X.; Tao, S. *Org. Electron.* **2020**, 83, 105747.
- (24) (a) Zabula, A. V.; Filatov, A. S.; Xia, J.; Jasti, R.; Petrukhina, M. A. *Angew. Chem. Int. Ed.* **2013**, 52, 5033. (b) Spisak, S. N.; Wei, Z.; Darzi, E.; Jasti, R.; Petrukhina, M. A. *Chem. Commun.* **2018**, 54, 7818. (c) Zhou, Z.; Wei, Z.; Schaub, T. A.; Jasti, R.; Petrukhina, M. A. *Chem. Sci.* **2020**, 11, 9395.
- (25) (a) Thordarson, P. *Chem. Soc. Rev.* **2011**, 40, 1305. (b) Hibbert, D. B.; Thordarson, P. *Chem. Commun.* **2016**, 52, 12792.
- (26) (a) Xia, Z.; Pun, S. H.; Chen, H.; Miao, Q. *Angew. Chem. Int. Ed.* **2021**, 60, 10311. (b) Wössner, J. S.; Wassy, D.; Weber, A.; Bovenkerk, M.; Hermann, M.; Schmidt, M.; Esser, B. *J. Am. Chem. Soc.* **2021**, 143, 12244.
- (27) Minameyer, M.; Xu, Y.; Frühwald, S.; Görling, A.; von Delius, M.; Drewello, T. *Chem. Eur. J.* **2020**, 26, 8729.
- (28) Considering that the nonpolar character of toluene prevents any electron transfer, we focused our measurements on THF, whose polarity is sufficient to power the electron transfer.
- (29) Fujitsuka, M.; Lu, C.; Zhuang, B.; Kayahara, E.; Yamago, S.; Majima, T. *J. Phys. Chem. A* **2019**, 123, 4737.
- (30) Fujitsuka, M.; Lu, C.; Iwamoto, T.; Kayahara, E.; Yamago, S.; Majima, T. *J. Phys. Chem. A* **2014**, 118, 4527.
- (31) Guldi, D. M.; Prato, M. *Acc. Chem. Res.* **2000**, 33, 695.
- (32) Reed, C. A.; Bolskar, R. D. *Chem. Rev.* **2000**, 100, 1075.
- (33) (a) Pérez, E. M.; Martín, N. *Chem. Soc. Rev.* **2015**, 44, 6425. (b) Zhang, B.; Hernández Sánchez, R.; Zhong, Y.; Ball, M.; Terban, M. W.; Paley, D.; Billinge, S. J. L.; Ng, F.; Steigerwald, M. L.; Nuckolls, C. *Nat. Commun.* **2018**, 9, 1957. (c) Miki, K.; Saiki, K.; Umeyama, T.; Baek, J.; Noda, T.; Imahori, H.; Sato, Y.; Suenaga, K.; Ohe, K. *Small* **2018**, 14, 1800720. (d) Barendt, T. A.; Ball, M. L.; Xu, Q.; Zhang, B.; Fowler, B.; Schattman, A.; Ritter, V. C.; Steigerwald, M.

L.; Nuckolls, C. *Chem. Eur. J.* **2020**, *26*, 3744. (e) Balakrishna, B.; Menon, A.; Cao, K.; Gsänger, S.; Beil, S. B.; Villalva, J.; Shyshov, O.; Martin, O.; Hirsch, A.; Meyer, B.; Kaiser, U.; Guldi, D. M.; von Delius, M. *Angew. Chem. Int. Ed.* **2020**, *59*, 18774. (f) Tanuma, Y.; Stergiou, A.; Bužan Bobnar, A.; Gaboardi, M.; Rio, J.; Volkmann, J.; Wegner, H. A.; Tagmatarchis, N.; Ewels, C. P.; Arčon, D. *Nanoscale* **2021**, *13*, 19946.